ACS APPLIED MATERIALS & INTERFACES

Research Article

www.acsami.org

Microstructure and Performance of Multiwalled Carbon Nanotube/*m*-Aramid Composite Films as Electric Heating Elements

Young Gyu Jeong*,† and Gil Woo Jeon‡

†Department of Advanced Organic Materials and Textile System Engineering, Chungnam National University, Daejeon 305-764, Republic of Korea

‡Department of Materials Design Engineering, Kumoh National Institute of Technology, Gumi, Gyeongbuk 730-701, Republic of Korea

Supporting Information

ABSTRACT: We report microstructure of thermomechanically stable multiwalled carbon nanotube (MWCNT)/poly(*m*-phenylene isophthalamide) (*m*-aramid) composite films containing 0.0−10.0 wt % MWCNTs and their performance as electric heating elements. FE-SEM images show that the MWCNTs are well dispersed in the composite films and are wrapped with *m*-aramid chains and that the interfacial thickness of *m*-aramid wrapped MWCNTs decreases with the MWCNT content. The electrical resistivity of films varies from ~10^{13} Ω cm for the neat *m*-aramid to ~10^{0} Ω cm of the film with 10.0 wt % MWCNT owing to the formation of a conductive three-dimensional network of MWCNTs. Accordingly, the performance of MWCNT/*m*-aramid films as electric heating elements is strongly dependent on MWCNT content as well as applied voltage. For the composite film with 10.0 wt % MWCNT, a maximum temperature of ~176 °C is attained even at a low applied voltage of 10 V. The excellent performance such as rapid temperature response and high electric power efficiency at given applied voltages is found to be related with the microstructural features of the MWCNT/*m*-aramid films.

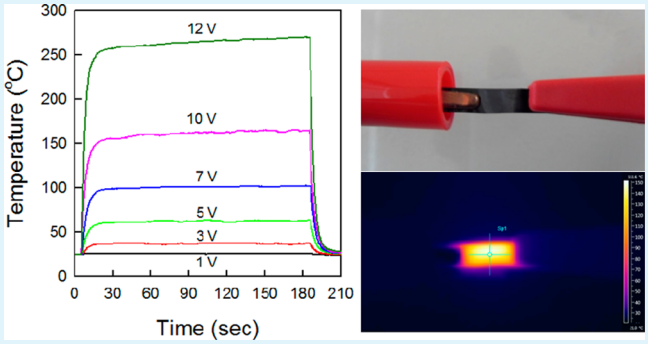

KEYWORDS: *carbon nanotubes, composite films, m-aramid, electric heating, electrical properties*

1. INTRODUCTION

Electrically conductive polymer composites including carbon nanotubes (CNTs) have generated a great deal of scientific and industrial interest,[1−3] since the discovery of CNTs with extraordinary mechanical property, thermal conductivity, thermal stability, and electrical conductivity of CNTs.[4,5] Generally, the electrical conductivity of CNT/polymer composites stems from the formation of a continuous network of conductive CNTs in an insulating polymer matrix.[6] Improvement in electrical conductivity of CNT/polymer composites has found significant applications in advanced areas such as pressure sensors,[7,8] temperature sensors,[9,10] selective gas/liquid sensors,[11,12] supercapacitors,[13,14] electrostatic dissipation (ESD), and electromagnetic interference (EMI) shielding materials for electronic devices and components.[15−17]

Electric heating materials or devices are also considered as high potential application areas for CNT/polymer composites.[9,18] They are a kind of electrical resistor that converts electrical energy into thermal energy as heat. Common applications of electric heating materials include plane heating, water heating, and industrial processes. Electric heating can be accurately applied at precise points with high concentration of power per unit area or volume. Advantages of electric heating methods over other forms include quietness, cleanness without emitting byproduct, precision control of ready achievable temperature, and uniform distribution of heat energy. In comparison to metallic materials used widely as electric heating materials owing to their high thermomechanical stability, electrically conductive polymer composites have additional advantages due to their lightweight, corrosion resistance, easy processing, and lower manufacturing cost. Therefore, electric heating films made of polymer composites can be built in any required size and can be located anywhere within a space. For practical applications, thermomechanical stability of electric heating elements or devices is also very important during the operation period. Therefore, a polymeric matrix with high thermal and mechanical stability is a prerequisite for CNT/polymer composites as electric heating materials.

Aramids, which are the general term of aromatic polyamides, are synthetic polymers possessing excellent thermal and oxidative stability, flame resistance, and superior mechanical properties.[19] Accordingly, they have found increasing uses in a wide variety of technical applications. One of these applications

Received: March 11, 2013
Accepted: June 25, 2013
Published: June 25, 2013

   dx.doi.org/10.1021/am400892k | ACS Appl. Mater. Interfaces 2013, 5, 6527−6534

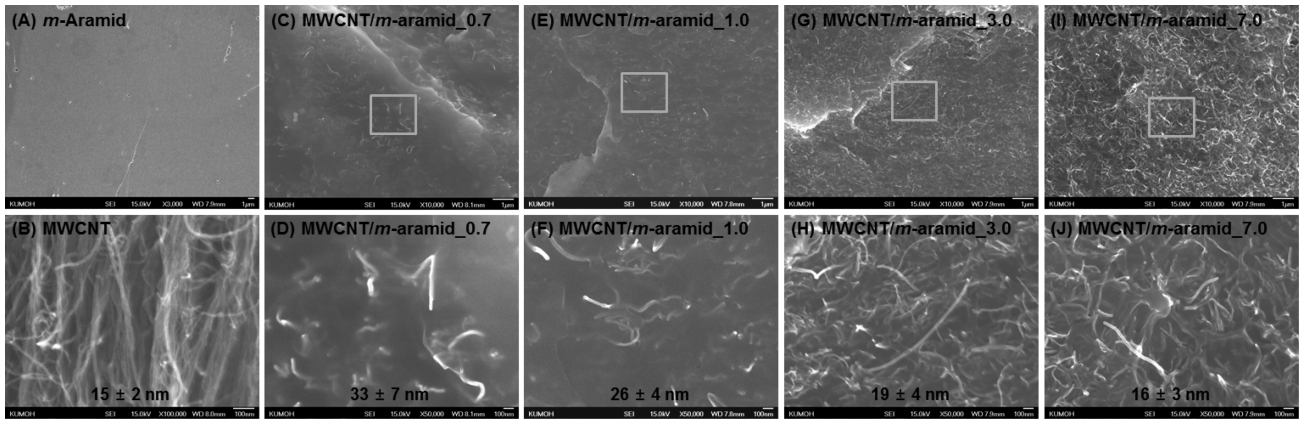

Figure 1. SEM images of pristine MWCNT and composite films with different MWCNT contents: (A) neat *m*-aramid; (B) pristine MWCNT; (C, D) MWCNT/*m*-aramid_0.7; (E, F) MWCNT/*m*-aramid_1.0; (G, H) MWCNT/*m*-aramid_3.0; (I, J) MWCNT/*m*-aramid_7.0.

takes advantage of their thermal stability and thus allows the manufacturing of heat-resistant materials for fire protection. Poly(*m*-phenylene isophthalamide) (*m*-aramid) and poly(*p*-phenylene terephthalamide) (*p*-aramid) are mostly well-known aramids and they have *meta*- and *para*-type benzene-amide linkages in the skeletal chains, respectively. Obviously, hydrogen bonding and chain rigidity of these aramids contribute to very high glass transition temperatures, which were measured to be 272 °C for *m*-aramid and 295 °C for *p*-aramid.[20] Since *m*- and *p*-aramids have high melting points or melt with decomposition because of the high rigidity and conjugation of the backbones, they are currently solution-processed into the forms of fibers, fibrids, pulps, films, papers, and particles. *m*-Aramid is easily dissolved in common organic solvents such as *N*,*N*-dimethylformamide (DMF), *N*,*N*-dimethylacetamide (DMAc), and *N*-methylpyrolidone (NMP) in the presence of inorganic salt, while *p*-aramid is soluble in strong acids and in highly polar solvents with inorganic salts. Therefore, *m*-aramid, which has many advantages such as easy processability using organic solvents, excellent thermal stability, and high mechanical property, is considered as an ideal polymeric matrix for fabricating electric heating films incorporating conductive CNTs.

In this study, we have investigated, for the first time, the performance of thermomechanically stable *m*-aramid composite films containing neat multiwalled carbon nanotube (MWCNT) as electric heating elements. For the purpose, a series of MWCNT/*m*-aramid composite films with various MWCNT contents of 0.0−10.0 wt % were prepared by a solution-casting method and their morphological feature, thermomechanical stability, and electrical resistivity were characterized. The performance of the composite films as electric heating elements was examined as functions of MWCNT content and applied voltage, and then it was analyzed in terms of temperature response rapidity, electric power efficiency, and operational stability.

2. EXPERIMENTAL SECTION

Pristine MWCNT (CM-250, Hanwha Nanotech Inc.) with 10−15 nm diameters and ∼100 μm length, which was produced by thermal chemical vapor deposition, was used as conductive reinforcing nanofiller. The elemental composition of the neat MWCNT carried out with an energy dispersive X-ray spectrometer was analyzed to be C:O:Fe = 90.91 ± 3.16/8.13 ± 2.60/0.96 ± 0.64 by wt %. *m*-Aramid (staple type, Sigma-Aldrich Inc.) with a density of 1.38 g/mL at 25 °C was used as a polymer matrix for the composite films. *N*,*N*-Dimethylacetamide (DMAc, Daejung Chemical & Metals Com.) and anhydrous lithium chloride (LiCl, Wako Chem.) were used as a solvent and a salt, respectively, for preparing MWCNT/*m*-aramid solutions. All the materials and chemicals were used as received without further purification.

MWCNT/*m*-aramid composite films were fabricated by a solution-casting method. First, DMAc solutions including 2 wt % LiCl were stirred on hot plates at 60 °C for 30 min. Then, 10 wt % *m*-aramid staples were added in DMAc/LiCl solutions and stirred at 80 °C for 12 h. Second, DMAc solutions containing different MWCNT contents (0.0−10.0 wt % of the *m*-aramid) were prepared and sonicated for 6 h by using a bath type sonicator (50−60 Hz). Third, each MWCNT/DMAc solution was added in *m*-aramid/DMAc/LiCl solutions and sonicated again for 6 h. The ultrasonication cycle of 1 min run and 9 min stop was repeated during all the sonication process. The MWCNT/*m*-aramid solutions were casted on glass plates, which were placed on hot plates at 80 °C for 24 h to evaporate DMAc solvent. Finally, neat *m*-aramid and its composite films on the glass plates were washed in distilled water at 80 °C for 3 h to remove residual DMAc solvent and were then dried in a vacuum oven at 160 °C for 12 h. The thickness of the final composite films was controlled to be ∼200 μm. The fabricated film samples were named to MWCNT/*m*-aramid_X, where X denotes the MWCNT content by wt %.

To identify the morphological feature and the dispersion state of MWCNTs in the composites, the film samples were cryogenically fractured in a liquid nitrogen bath and their fractured surfaces were characterized by using a field-emission scanning electron microscope (FE-SEM, JEOL/JSM-6701F) equipped with an energy dispersive X-ray spectrometer (EDS). Dynamic mechanical thermal properties of the MWCNT/*m*-aramid composite films were examined with the aid of a dynamic mechanical analyzer (DMA, TA Q800) under the tensile mode from 50 to 400 °C at a heating rate of 5 °C/min and a frequency of 1 Hz. Thermal stability of the composite films was also investigated by using a thermomechanical analyzer (TGA, TA Q100) under the air condition at a heating rate of 10 °C/min. Electrical current (I) of the composite films with different MWCNT contents was measured as a function of applied voltage (V) by using multiple sourcemeters and ohmmeters (6517A, 2400, 2182A, Keithley Instruments Inc.). Electric heating behavior of the composite films under a variety of applied voltages of 1−100 V was characterized with an infrared camera (SE/A325, FLIR Systems Inc.) and a sourcemeter (2400, Keithley Instruments Inc.). For the electrical experiments, film samples with 5.0 mm width and 40.0 mm length were prepared. In the case of the electrical measurement, the distance between electrical test probes was kept at 10.0 mm.

3. RESULTS AND DISCUSSION

3.1. Microstructural Feature. Figure 1 show FE-SEM images of pristine MWCNT, *m*-aramid, and composite films with different MWCNT contents. The fractured surface of the neat *m*-aramid is very clean and smooth without showing any micropores (Figure 1A), which supports that the solution-casting process is quite efficient for manufacturing *m*-aramid and its composite films. FE-SEM image also confirms that pristine MWCNT used as the conductive filler has the average diameter of 15 ± 2 nm and the high aspect ratio of ∼1000 (Figure 1B). In the cases of the composite films, MWCNTs were found to be uniformly and randomly dispersed in the *m*-aramid matrix (Figure 1C–J). Interestingly, it was identified that the apparent average diameter of MWCNTs dispersed in the composite films was even higher than that of the neat MWCNT, although it decreased with increasing the MWCNT content in the composite films. For instance, the apparent average diameter of MWCNTs in MWCNT/*m*-aramid_0.7 was evaluated to be 33 ± 7 nm (Figure 1D). It demonstrates that MWCNTs in the composite films are physically coated with *m*-aramid chains during the ultrasonication-assisted solution process. Therefore, for MWCNT/*m*-aramid_0.7, the interfacial thickness by *m*-aramid chains can be evaluated to be ∼18 nm by comparing the apparent average diameter of MWCNTs in the composite film with the value of neat MWCNTs. This interfacial thickness of *m*-aramid wrapped MWCNTs were thinner with increasing the MWCNT content in the composite films: ∼11 nm for MWCNT/*m*-aramid_1.0 (Figure 1F), ∼4 nm for MWCNT/*m*-aramid_3.0 (Figure 1H), and ∼1 nm for MWCNT/*m*-aramid_7.0 (Figure 1J). It has been recently reported that the interdistance among CNTs in composite matrices should be small enough for the efficient tunneling of electrons through CNT/polymer composites.[21−23] It is thus expected that the MWCNT content as well as the interfacial thickness influences strongly the electrical conductivity and electric heating behavior of MWCNT/*m*-aramid composite films, as will be discussed below.

3.2. Thermal Stability. Dynamic mechanical and thermal properties of MWCNT/*m*-aramid composite films with different MWCNT contents were examined in a wide temperature range of 50−400 °C. As a result, changes of dynamic storage modulus (E') with temperature were presented in Figure 2A. For the neat *m*-aramid film, the storage modulus remained constant at the glassy region, decreased dramatically at ∼270 °C owing to the glass-to-rubber transition, decreased again at ∼325 °C due to the rubber-to-flow transition, and increased slightly at ∼370 °C by the volume shrinkage of *m*-aramid starting with partial thermal degradation (Figure 2A). These characteristic thermal transition regimes were assigned by comparing the dynamic mechanical data of Figure 2 with the glass transition temperature and thermal degradation behavior of *m*-aramid reported in literature.[20,24] In cases of the composite films, the storage moduli up to the glass transition region were quite comparable with the neat *m*-aramid film, whereas the moduli at the rubbery region became higher with increasing the MWCNT content and the rubber-to-flow transition was not detected for the composite films with high MWCNT contents of 5.0 and 10.0 wt % due to the reinforcing effect of MWCNTs. It has been reported that the thermal degradation of *m*-aramid begins with the cleavage of the hydrogen bonds at ∼360 °C and happens dominantly at 400−600 °C with the disruption of the amide bonds.[24] It was found

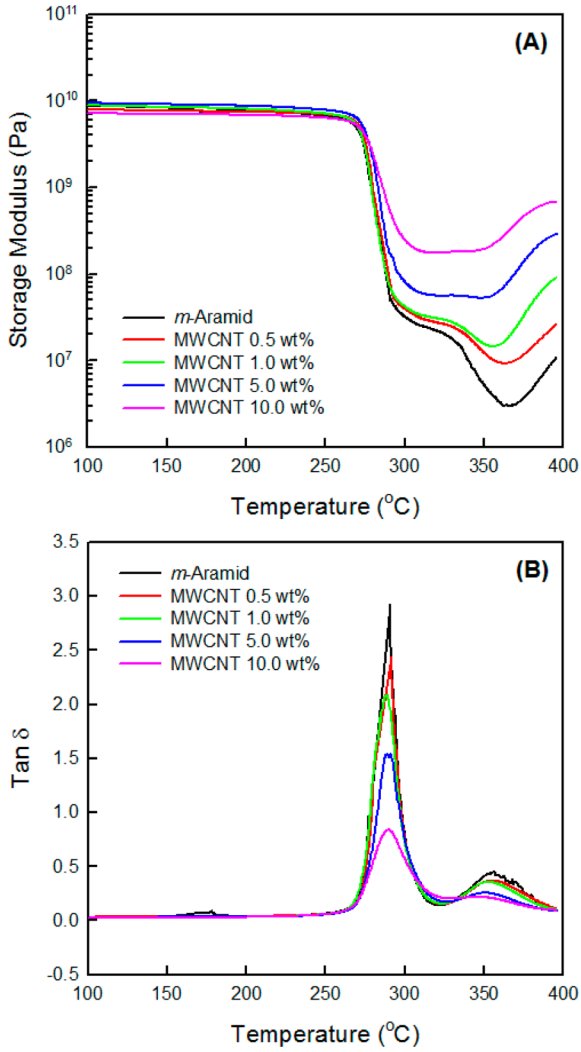

Figure 2. (A) Dynamic storage modulus and (B) tan δ of the neat *m*-aramid and its composite films with different MWCNT contents as a function of temperature.

that the thermal degradation behavior of MWCNT/*m*-aramid composite films was quite consistent with that of the neat *m*-aramid film within experimental error (Supporting Information Figure S1).

The loss tangent (tan δ) versus temperature curves exhibit two dominant relaxation peaks, as shown in Figure 2B. The first strong peak at ∼290 °C, which originates from the α-relaxation of *m*-aramid backbone, is associated with the glass transition temperature (T_g). Although the peak glass transition temperature is almost identical, irrespective of the MWCNT content in the composite films, the peak became weaker and broader with the increment of the MWCNT content. This result is caused by the presence of MWCNTs wrapped with *m*-aramid and dispersed uniformly in the composite films, which leads to restraining the mobility of *m*-aramid chains in the glass transition. On the other hand, the second weak peak at ∼355 °C, which stems from the rubber-to-flow transition of *m*-aramid chains, became weaker with increasing the MWCNT content in the composite films and it disappeared for the composite film with high MWCNT content of 10 wt % owing to the reinforcing effect of MWCNTs at the high temperature range.

3.3. Electrical Properties. Electrical properties of MWCNT/*m*-aramid composite films were investigated as

dx.doi.org/10.1021/am400892k | ACS Appl. Mater. Interfaces 2013, 5, 6527−6534

functions of MWCNT content and applied voltage. Figure 3 presents current−voltage (I−V) curves of the composite films

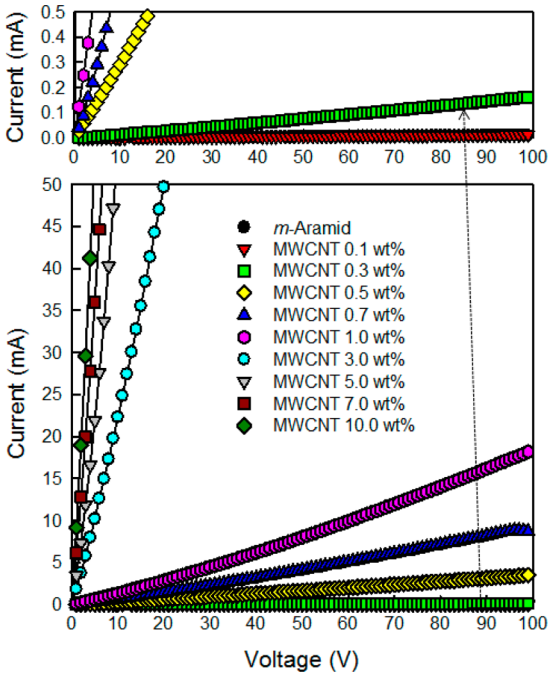

Figure 3. Current−voltage (I−V) curves for neat *m*-aramid and its composite films with different MWCNT contents.

containing different MWCNT contents. For the neat *m*-aramid and the composite films with 0.1 and 0.3 wt % MWCNTs, no electrical current was detected over the applied voltage range of 1−100 V. It is explained by the fact that, for the composite films with low MWCNT contents of 0.1 and 0.3 wt %, the interdistance among MWCNTs dispersed uniformly in the composite films and wrapped by *m*-aramid chains are not close enough for the electron tunneling.[25] On the other hand, the electrical current of the composite films with MWCNT contents of 0.5−10.0 wt % increased linearly with the applied voltage and the slopes of the I−V curves were steeper for the composite film with higher MWCNT content. It demonstrates that the electrical transport properties of MWCNT/*m*-aramid composite films with 0.5−10.0 wt % MWCNTs exhibit linear behavior by obeying Ohm's law.

The electrical resistance (R) of MWCNT/*m*-aramid composite films was evaluated from the slopes of I−V curves in Figure 3 and it was plotted as a function of MWCNT content, as shown in Figure 4. By using the relation of $R = \rho(L/A)$, where L is the sample length between electrodes and A is the cross-sectional area of a film sample, the electrical resistivity (ρ) of the composite films could be calculated and the result was also presented as a function of MWCNT content, as can be seen in Figure 4. The electrical resistivity was strongly dependent on MWCNT content by showing a typical percolation behavior. It was found that the electrical resistivity decreased dramatically from $\sim 10^{13}$ Ω cm for the neat *m*-aramid to $\sim 10^{0}$ Ω cm for the composite with 10.0 wt % MWCNT. Especially, it appeared that the electrical percolation threshold was formed at certain MWCNT content between 0.0 and 0.1 wt %. It is generally accepted that, when the CNT content reaches the electrical percolation threshold, a conductive path owing to the network of CNTs forms in the composite

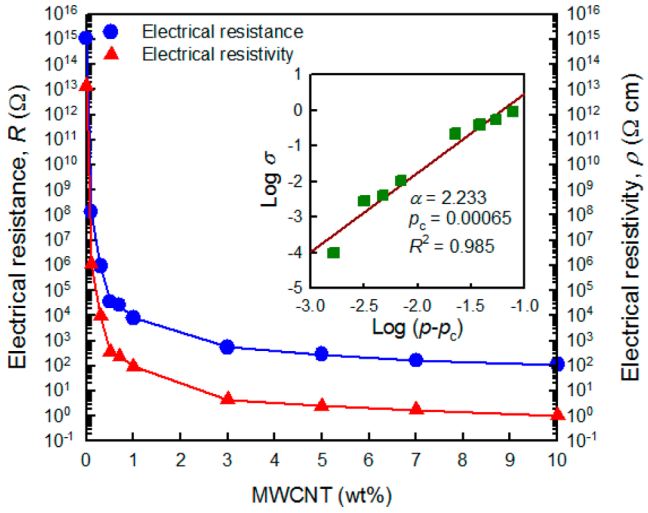

Figure 4. Electrical resistance and resistivity of MWCNT/*m*-aramid composite films as a function of the MWCNT content. Inset is a log−log plot of electrical conductivity versus volume fraction of MWCNT.

matrix.[6,25−27] To determine the electrical percolation threshold, the following power law relation can be used[28,29]

$$\sigma \propto (p - p_c)^{\alpha} \quad (1)$$

where σ is the electrical conductivity (the inverse of electrical resistivity), p is the MWCNT volume fraction, p_c is the critical volume fraction at electrical percolation, and α is the critical exponent. The straight line with p_c = 0.00065 (~0.085 wt %) and α = 2.233 gives a good fit to the experimental data of log σ versus log($p - p_c$) (inset of Figure 4). The critical exponent provides an index of the system dimensionality, and theoretical values of 1.3 and 1.94 have been predicted for ideal 2-D and 3-D systems, respectively.[28] Thus, the α value of 2.233 for the MWCNT/*m*-aramid composite films indicates that MWCNTs form a quasi-3-D network at the percolation threshold of ~0.085 wt % MWCNT. In addition, it is speculated that the low p_c value of ~0.085 wt % MWCNT arises from the uniform and random dispersion of MWCNTs in the *m*-aramid matrix. For the composite films with high MWCNT of 3.0−10.0 wt %, quite low electrical resistivity of ~10° Ω cm was attained. This low electrical resistivity of MWCNT/*m*-aramid composite films is strongly related with the morphological feature. As discussed above, for the composite films with higher MWCNT contents, MWCNTs are more densely dispersed in the *m*-aramid matrix and the interfacial thickness of *m*-aramid wrapped MWCNTs are also even thinner, which results in facilitating the electron tunneling among MWCNTs for the efficient electrical conduction. On the other hand, it should be mentioned that the MWCNT/*m*-aramid composite films with low electrical resistivity less than $\sim 10^{8}$ Ω cm can be utilized as ESD and/or EMI shielding materials for electronic devices and components.

3.4. Electric Heating Behavior. Electric heating experiments of *m*-aramid composite films with different MWCNT contents were carried out by varying applied voltages of 1−100 V. Figure 5A and B shows representative digital images of MWCNT/*m*-aramid_1.0 for the characterization of electric heating behavior. It can be seen that the composite film with 1.0 wt % MWCNT is highly flexible (Figure 5A), which originates from the good dispersion of MWCNTs with high aspect ratio in the *m*-aramid matrix. For electric heating experiments, the distance between two electrodes was kept to

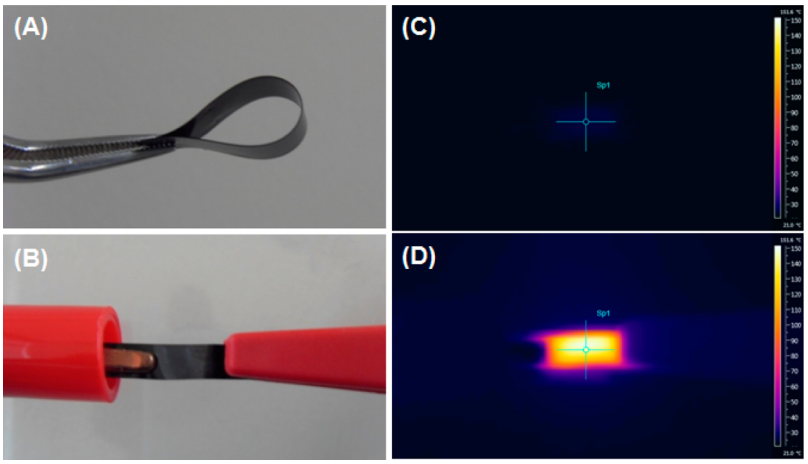

Figure 5. (A) Digital image of MWCNT/*m*-aramid_1.0 composite film in bending. (B) Digital image of MWCNT/*m*-aramid_1.0 composite film with electrodes for the electric heating experiment. (C, D) Infrared thermal images of MWCNT/*m*-aramid_1.0 composite film before and after applying a voltage.

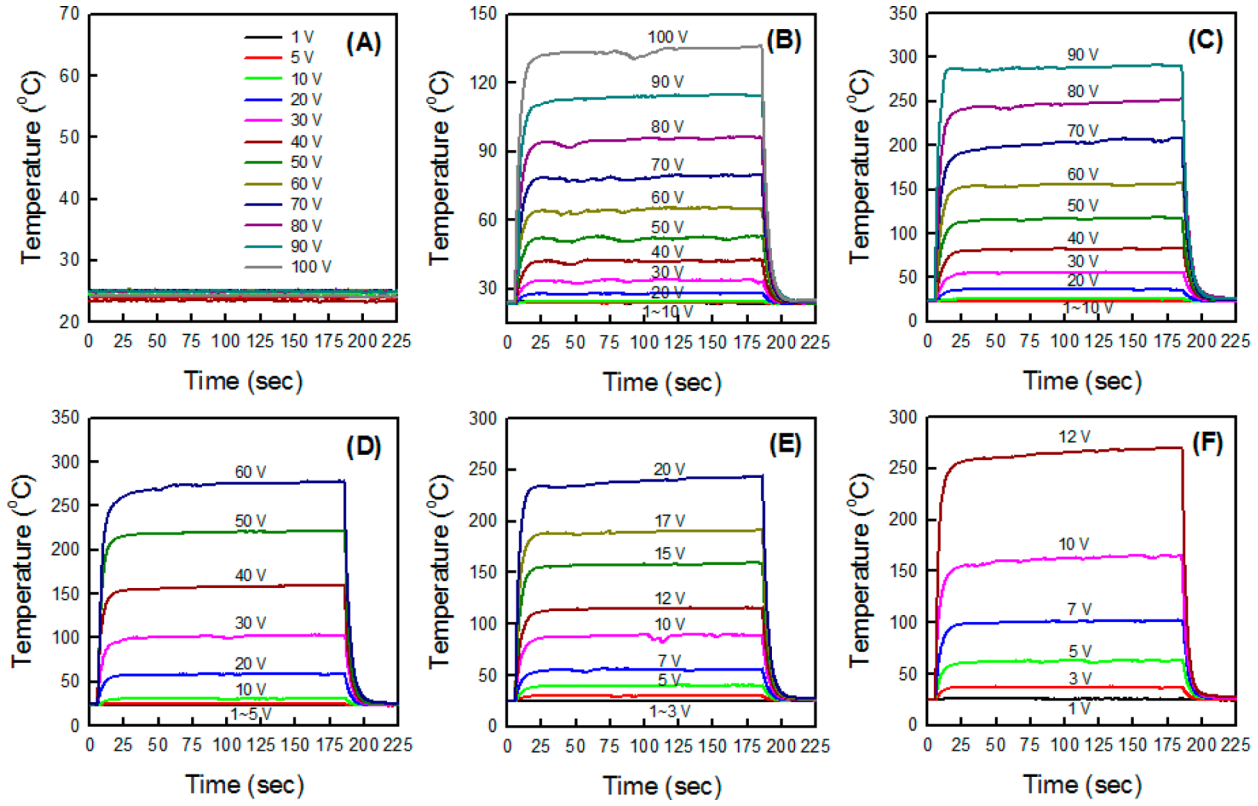

Figure 6. Time-dependent temperature changes of MWCNT/*m*-aramid composite films at different applied voltages of 1−100 V: (A) MWCNT/*m*-aramid_0.3; (B) MWCNT/*m*-aramid_0.5; (C) MWCNT/*m*-aramid_0.7; (D) MWCNT/*m*-aramid _1.0; (E) MWCNT/*m*-aramid_7.0; (F) MWCNT/*m*-aramid_10.0.

be 10 mm (Figure 5B). Infrared images of MWCNT/*m*-aramid_1.0 before and after applying a voltage are shown in Figure 5C and D, respectively. When a voltage was applied, the infrared image of the composite film changed from black to bright yellow to white with time, which confirms the existence of the electric heating behavior. It was found that the electric heating behavior of MWCNT/*m*-aramid composite films was strongly dependent on the MWCNT content as well as the applied voltage. Figure 6 presents the time-dependent temperature changes of the composite films with 0.3−10.0 wt % MWCNTs at various applied voltages. In the cases of the neat *m*-aramid and composite films with low MWCNT contents of 0.1 and 0.3 wt %, no temperature changes were observed over the applied voltages of 1−100 V, which indicates that there was no electric heating behavior (Figure 6A). For MWCNT/*m*-aramid_0.5, the temperature increased rapidly when a voltage above ∼20 V was applied at 5 s, reached a maximum value within ∼30 s, and decreased quickly to room temperature when the applied voltage was off at 185 s (Figure 6B). The maximum temperature was found to increase with the increment of the applied voltage. This electric heating behavior was also detected for other composite films with higher MWCNT contents of

dx.doi.org/10.1021/am400892k | ACS Appl. Mater. Interfaces 2013, 5, 6527−6534

Table 1. Characteristic Parameters (τ_g, τ_d, and h_{r+c}) for Electric Heating Performance of MWCNT/*m*-Aramid Composite Films under Applied Voltages

sample code	voltage (V)	τ_g (s)	τ_d (s)	h_{r+c} (mW/°C)
MWCNT/*m*-aramid_0.5	20−100	6.45 ± 0.87	9.34 ± 2.22	2.8 ± 0.3
MWCNT/*m*-aramid_0.7	20−100	4.30 ± 1.44	9.23 ± 0.84	2.2 ± 0.3
MWCNT/*m*-aramid_1.0	10−60	5.75 ± 1.06	8.91 ± 1.91	4.2 ± 0.2
MWCNT/*m*-aramid_3.0	5−20	4.35 ± 0.83	12.61 ± 2.68	5.6 ± 0.6
MWCNT/*m*-aramid_5.0	3−20	4.53 ± 0.57	11.62 ± 2.92	9.9 ± 0.9
MWCNT/*m*-aramid_7.0	3−20	4.62 ± 0.91	9.98 ± 0.77	13.8 ± 2.6
MWCNT/*m*-aramid_10.0	3−12	4.69 ± 0.38	10.39 ± 1.02	7.4 ± 0.8

0.7−10.0 wt %, except the result that the maximum temperatures at different applied voltages were even higher for the composite films with higher MWCNT contents (Figure 6C−F).

Time-dependent temperature curves in Figure 6B−F can be divided into three regions: the temperature growth (heating) region (5−30 s), the equilibrium (maximum temperature) region (30−185 s), and the temperature decay (cooling) region (185−225 s). In the first region, the temperature growth with time can be empirically expressed as[18,30,31]

$$\left(\frac{T_t - T_0}{T_m - T_0}\right) = 1 - e^{-t/\tau_g} \quad (2)$$

where T_0 and T_m are the initial and maximum temperature, respectively. T_t is an arbitrary temperature at time t. τ_g is the characteristic growth time constant. For all the composite films showing electric heating behavior, the τ_g values could be calculated by fitting the data in the first stage of temperature versus time plots in Figure 6, and they are listed in Table 1. It was found that the τ_g values were not dependent on the MWCNT content within the experimental error. On the other hand, the average τ_g value of 4.97 ± 1.21 s for all the composite films is far lower than the ones for inorganic filler-reinforced polymer composites reported in literature.[18,30,31] It indicates that MWCNT/*m*-aramid composite films exhibit unusually rapid temperature responses to applied voltages.

In the second region in equilibrium, heat gain by electric power is equal to heat loss by radiation and convection according to the conservation law of energy. The heat transferred by radiation and convection, h_{r+c}, is expressed as

$$h_{r+c} = \frac{I_c V_0}{T_m - T_0} \quad (3)$$

where I_c is the steady state current and V_0 is the initial applied voltage. Accordingly, the h_{r+c} values could be calculated, as summarized in Table 1. The h_{r+c} values were generally higher for the composite films with higher MWCNT contents. In addition, the average h_{r+c} value of 6.5 ± 4.3 mW/°C for all the composite films is quite lower than the values reported for other polymer composite systems,[18,30,31] which demonstrates that MWCNT/*m*-aramid composite films have high electric heating efficiency by requiring relatively low electric power to maintain a maximum temperature.

In the last region, during which the applied voltage was off, the composite films were left to cool down by radiation and convection according to Newton's law of cooling. Therefore, the temperature decreases with time, which can be described by the following empirical formula:

$$\left(\frac{T_t - T_0}{T_m - T_0}\right) = e^{-t/\tau_d} \quad (4)$$

where τ_d is the decay time constant. The τ_d values were calculated by fitting temperature decay data with time in Figure 6, and they are also listed in Table 1. For all the composite films with 0.5−10.0 wt % MWCNT, the average τ_d value was estimated to be 10.26 ± 2.24 s, which also supports that MWCNT/*m*-aramid composite films show efficient cooling behavior.

The maximum temperatures (T_{max}) of the composite films with 0.5−10.0 wt % MWCNTs were found to increase nonlinearly with the applied voltage, as shown in Figure 7.

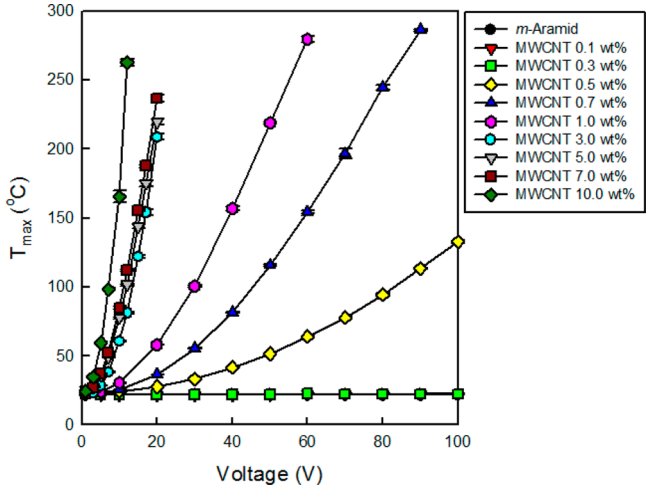

Figure 7. Changes of maximum temperature (T_{max}) of MWCNT/*m*-aramid composite films with different MWCNT contents as a function of the applied voltage.

On the other hand, it should be noted that T_{max} values for the composite films with high MWCNT contents of 3.0−10.0 wt % increased steeply at the narrow applied voltage range of 1−20 V. This result is believed to be associated with the low electrical resistivity of ~10° Ω cm for the composite films with 3.0−10.0 wt % MWCNTs, unlike other composite films with relatively low MWCNTs of 0.1−1.0 wt %.

The electric power (P) associated with the flow of a current (I) under an applied voltage (V) is given by $P = VI$. In combination with Ohm's law of $V = IR$, the electric power is also expressed as

$$P = \frac{V^2}{R} \quad (5)$$

where the electric power is quadratically proportional to the voltage. This electric power is dissipated as heat, thus allowing a

dx.doi.org/10.1021/am400892k | ACS Appl. Mater. Interfaces 2013, 5, 6527−6534

form of heating known as resistance heating or Joule heating. For all MWCNT/*m*-aramid composite films, changes of the experimental electric power with the applied voltage are represented in Figure 8. It was found that, for the composite

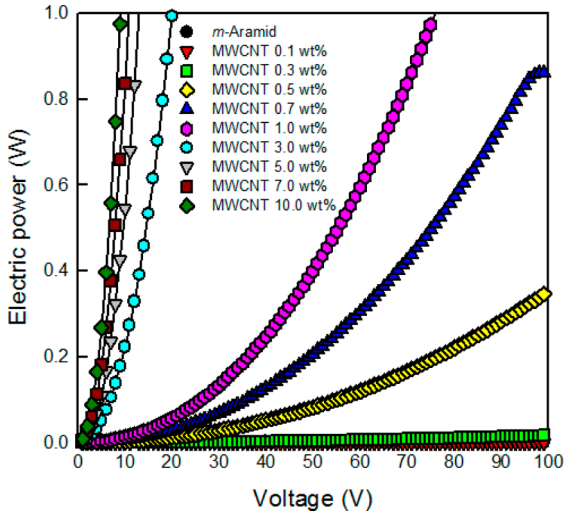

Figure 8. Changes of electric power of MWCNT/*m*-aramid composite films with different MWCNT contents as a function of the applied voltage.

films with 0.3−10.0 wt % MWCNTs, the electric power increased quadratically with respect to the applied voltage. It means that MWCNT/*m*-aramid composite films showing electric heating behavior can serve as a classical ohmic conductor. Since the electric power is associated with the transduction of electrical energy into Joule heating, it is reasonable to contend that the quadratic increment of the maximum temperature with the applied voltage (Figure 7) is related with the quadratic increasing trend of electric power (Figure 8). It should be mentioned that the experimentally measured electric power of Figure 8 was quite consistent with the power calculated from the eq 5 using the electrical resistance of Figure 3 within the % deviation of 0.01−10.51%.

The operational stability of MWCNT/*m*-aramid composite film as an electric heater was investigated by performing heating−cooling cycles. Figure 9 shows the temperature

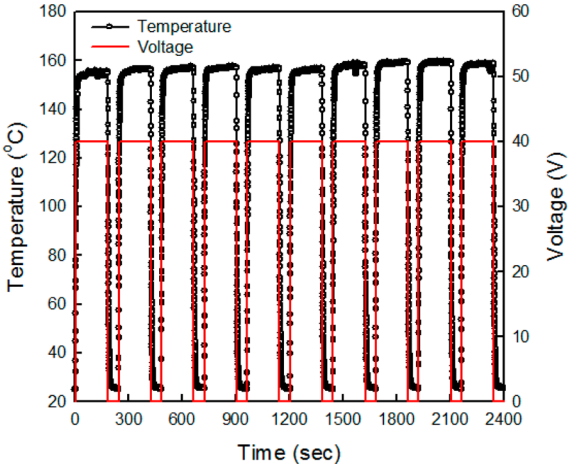

Figure 9. Temperature response of MWCNT/*m*-aramid_1.0 under a cyclic voltage change.

response of MWCNT/*m*-aramid_1.0 under a cyclic voltage of 40 V. It was found that, over the cyclic applied voltage, the heating and cooling behavior as well as the maximum temperature of ∼155 °C remained constant without any structural change of the composite film, which was due to the excellent thermomechanical stability of *m*-aramid matrix with the high glass transition temperature of ∼290 °C. It should be mentioned that there was no noticeable structural change for MWCNT/*m*-aramid_1.0 films before and after the heating−cooling cyclic experiments of Figure 9.

4. CONCLUSIONS

We have prepared MWCNT/*m*-aramid composite films with various neat MWCNT contents by a simple and efficient solution-casting method and investigated their performance as electric heating elements by correlating with microstructure and electrical resistivity. It was identified from FE-SEM images that neat MWCNTs are well dispersed in the *m*-aramid matrix and that the interfacial thickness of *m*-aramid wrapped MWCNTs decreased with the increment of MWCNT content in the composite films. The electrical resistivity of the composite films changed considerably with the MWCNT content from $\sim 10^{13}$ Ω cm for neat *m*-aramid film to $\sim 10^{0}$ Ω cm for MWCNT/*m*-aramid_10.0. The electrical percolation threshold was evaluated to be ∼0.085 wt % MWCNT, above which MWCNTs formed 3-D networks in the *m*-aramid matrix. Accordingly, the performance of the composite films as electric heating elements was strongly dependent on MWCNT content as well as applied voltage. The composite films with low MWCNT contents of 0.1−0.3 wt % did not display electric heating behavior, while the composite films with 0.5−10.0 wt % MWCNTs exhibited excellent electric heating behavior such as rapid temperature response and low electric power to maintain a maximum temperature at a given applied voltage. Higher maximum temperature at a constant applied voltage was attained for the composite films with higher MWCNT content. In addition, high operational stability in the electric heating for the composite films was also confirmed. Overall, it is valid to conclude that the excellent performance of the MWCNT/*m*-aramid composite films as electric heating elements is caused by the good dispersion of conductive MWCNTs wrapped by the *m*-aramid chains. Dynamic mechanical and thermal analyses of the MWCNT/*m*-aramid composite films supported that there were no noticeable changes in storage modulus up to the onset glass transition temperature of ∼270 °C. Accordingly, the MWCNT/*m*-aramid composite films can be thus utilized as electric heating elements or devices without emitting electromagnetic waves harmful to humans and electronic devices in various advanced applications such as floor heating, mirror/window defrosting, road deicing, oil/solution heating, medical instruments, and functional textiles, which do not require high temperatures above 100 °C, since the exact maximum temperatures of the composite films can be controlled by varying MWCNT contents as well as applied voltages. In addition, the composite films with low electrical resistivity of 10^{0}−10^{8} Ω cm can be also employed as ESD and/or EMI shielding materials.

■ ASSOCIATED CONTENT

Ⓢ Supporting Information

TGA curves. This material is available free of charge via the Internet at http://pubs.acs.org.

AUTHOR INFORMATION

Corresponding Author

*Tel: +82-42-821-6617. E-mail: ygjeong@cnu.ac.kr.

Notes

The authors declare no competing financial interest.

ACKNOWLEDGMENTS

This work was supported by the National Research Foundation of Korea (NRF) Grant funded by the Korean Government(-MOE)(2013R1A1A2A10010080).

REFERENCES

(1) Thostenson, E. T.; Ren, Z.; Chou, T.-W. *Compos. Sci. Technol.* **2001**, *61*, 1899−1912.
(2) Moniruzzaman, M.; Winey, K. I. *Macromolecules* **2006**, *39*, 5194−5205.
(3) Coleman, J. N.; Khan, U.; Blau, W. J.; Gun'ko, Y. K. *Carbon* **2006**, *44*, 1624−1652.
(4) Treacy, M. M. J.; Ebbesen, T. W.; Gibson, J. M. *Nature* **1996**, *381*, 678−680.
(5) Ebbesen, T. W.; Lezec, H. J.; Hiura, H.; Bennett, J. W.; Ghaemi, H. F.; Thio, T. *Nature* **1996**, *382*, 54−56.
(6) Du, F.; Scogna, R. C.; Zhou, W.; Brand, S.; Fischer, J. E.; Winey, K. I. *Macromolecules* **2004**, *37*, 9048−9055.
(7) Mohiuddin, M.; Hoa, S. V. *Nanoscale Res. Lett.* **2011**, *6*, 419.
(8) Hwang, J.; Jang, J.; Hong, K.; Kim, K. N.; Han, J. H.; Shin, K.; Park, C. E. *Carbon* **2011**, *49*, 106−110.
(9) Neitzert, H. C.; Vertuccino, L.; Sorrentino, A. *IEEE Trans. Nanotechnol.* **2011**, *10*, 688−693.
(10) Han, Z.; Fina, A. *Prog. Polym. Sci.* **2011**, *36*, 914−944.
(11) Li, L.; Yang, Z. B.; Gao, H. J.; Zhang, H.; Ren, J.; Sun, X. M.; Chen, T.; Kia, H. C.; Peng, H. S. *Adv. Mater.* **2011**, *23*, 3730−3735.
(12) Potschke, P.; Kobashi, K.; Villmow, T.; Andres, T.; Paiva, M. C.; Covas, J. A. *Compos. Sci. Technol.* **2011**, *71*, 1451−1460.
(13) Frackowiak, E.; Khomenko, V.; Jurewicz, K.; Lota, K.; Beguin, F. *J. Power Sources* **2006**, *153*, 413−418.
(14) Pan, H.; Li, J. Y.; Feng, Y. P. *Nanoscale Res. Lett.* **2010**, *5*, 654−668.
(15) Thomassin, J.-M.; Lou, X.; Pagnoulle, C.; Saib, A.; Bednarz, L.; Huynen, I.; Jerome, R.; Detrembleur, C. *J. Phys. Chem. C* **2007**, *111*, 11186−11192.
(16) Al-Saleh, M. H.; Sundararaj, U. *Carbon* **2009**, *47*, 1738−1746.
(17) Lee, J. I.; Yang, S. B.; Jung, H. T. *Macromolecules* **2009**, *42*, 8328−8334.
(18) Isaji, S.; Bin, Y.; Matsuo, M. *Polymer* **2009**, *50*, 1046−1053.
(19) Gabara, V.; Hartzler, J. D.; Lee, K.-S.; Rodini, D. J.; Yang, H. H. Aramid fibers. In *Handbook of Fiber Chemistry*, 3rd ed.; Lewin, M., Ed.; CRC Press: Boca Raton, FL, 2007.
(20) Aharoni, S. M.; Curran, S. A.; Murthy, N. S. *Macromolecules* **1992**, *25*, 4431−4436.
(21) Li, C.; Thostenson, E. T.; Chou, T.-W. *Appl. Phys. Lett.* **2007**, *91*, 223114.
(22) Yu, Y.; Song, G.; Sun, L. *J. Appl. Phys.* **2010**, *108*, 084319.
(23) Takada, T.; Shindo, Y.; Kuronuma, Y.; Narita, F. *Polymer* **2011**, *52*, 3852−3856.
(24) Villar-Rodil, S.; Paredes, J. I.; Martinez-Alonso, A.; Tascon, J. M. D. *Chem. Mater.* **2001**, *13*, 4297−4304.
(25) Hu, N.; Karube, Y.; Yan, C.; Masuda, Z.; Fukunaga, H. *Acta Mater.* **2008**, *56*, 2929−2936.
(26) Hu, N.; Masuda, Z.; Yan, C.; Yamamoto, G.; Fukunaga, H.; Hashida, T. *Nanotechnology* **2008**, *19*, 215701.
(27) Njuguna, M. K.; Yan, C.; Hu, N.; Bell, J. M.; Yariagadda, P. K. D. V. *Composites, Part B* **2012**, *43*, 2711−2717.
(28) Stauffer, D.; Aharon, A. *Introduction to percholation theory*, revised 2nd ed.; CRC Press: London and Philadelphia, 1994.
(29) Benoit, J. M.; Corraze, B.; Chauvet, O. *Phys. Rev. B* **2002**, *65*, 24140501−24140504.
(30) El-Tantawy, F. *Eur. Polym. J.* **2001**, *37*, 565−574.
(31) El-Tantawy, F.; Kamada, K.; Ohnabe, H. *Mater. Lett.* **2002**, *56*, 112−126.